

A LOW-COMPLEXITY STRUCTURED NEURAL NETWORK TO REALIZE STATES OF DYNAMICAL SYSTEMS*

HANSAKA ALUVIHARE[†], LEVI LINGSCH[‡], XIANQI LI[§], AND SIRANI M. PERERA[¶]

Abstract. Data-driven learning is rapidly evolving and places a new perspective on realizing state-space dynamical systems. However, dynamical systems derived from nonlinear ordinary differential equations (ODEs) suffer from limitations in computational efficiency. Thus, this paper stems from data-driven learning to advance states of dynamical systems utilizing a structured neural network (StNN). The proposed learning technique also seeks to identify an optimal, low-complexity operator to solve dynamical systems, the so-called Hankel operator, derived from time-delay measurements. Thus, we utilize the StNN based on the Hankel operator to solve dynamical systems as an alternative to existing data-driven techniques. We show that the proposed StNN reduces the number of parameters and computational complexity compared with the conventional neural networks and also with the classical data-driven techniques, such as Sparse Identification of Nonlinear Dynamics (SINDy) and Hankel Alternative view of Koopman (HAVOK), which is commonly known as delay-Dynamic Mode Decomposition(DMD) or Hankel-DMD. More specifically, we present numerical simulations to solve dynamical systems utilizing the StNN based on the Hankel operator beginning from the fundamental Lotka-Volterra model, where we compare the StNN with the LEarning Across Dynamical Systems (LEADS), and extend our analysis to highly nonlinear and chaotic Lorenz systems, comparing the StNN with conventional neural networks, SINDy, and HAVOK. Hence, we show that the proposed StNN paves the way for realizing state-space dynamical systems with a low-complexity learning algorithm, enabling prediction and understanding of future states.

Key words. Dynamical systems, Neural Networks, Operator Learning, Data-driven Algorithms, Low-complexity Algorithms, Performance of Learning Algorithms, Nonlinear ODEs

AMS subject classifications. 34N05, 37L05, 65L20, 65Y20, 68T07, 68T07

1. Introduction. Mathematical models can be utilized to continually analyze the dynamics of system states, providing a unique tool to represent dynamical systems. These models are formulated through a set of rules, often expressed as differential or difference equations, which dictate how the state variables evolve through time in continuous or discrete settings. Describing the evolution of state variables over time is a key aspect of solving dynamical systems. Depending on the system's complexity and continuity, one could achieve this while analytically solving the systems. Various methods can be used to analyze the solutions for continuous dynamical systems. These include separating variables for simple systems, linearizing to approximate nonlinear systems, spectral analysis, employing phase plane, and utilizing Laplace or Fourier transformations to obtain efficient solutions [18, 20, 27, 46]. These techniques provide a comprehensive understanding of the behavior and characteristics of dynamical systems. On the other hand, numerical techniques such as Euler's method, Runge-Kutta method, finite difference, finite element method, and spectral analysis are well-known to be applied to solve dynamical systems using iterative formulas [3, 44].

*Submitted to the editors February 26, 2025.

Funding: This work was funded by the Division of Mathematical Sciences, National Science Foundation with the award numbers 2410676 & 2410678.

[†]Department of Mathematics, Embry-Riddle Aeronautical University, Daytona Beach, FL, USA (aluvihah@my.erau.edu).

[‡]Seminar for Applied Mathematics, ETH Zurich, Zurich, Switzerland (levi.lingsch@sam.math.ethz.ch).

[§]Department of Mathematics & Systems Engineering, Florida Institute of Technology, Melbourne, FL, USA (xli@fit.edu).

[¶]Department of Mathematics, Embry-Riddle Aeronautical University, Daytona Beach, FL, USA (pereras2@erau.edu).

The exponential growth in data science places a new perspective on realizing state-space dynamical systems through data-driven approaches [12, 42]. With this said, dynamic mode decomposition (DMD) and extended DMD are utilized to identify the spatiotemporal structure of the high-dimensional data incorporating SVD through dimension reduction [29]. The DMD offers a modal decomposition, in which each mode is composed of spatially correlated structures that exhibit identical linear behavior over time. Thus, DMD not only reduces dimensions by using a smaller set of modes but also provides a model for the evolution of these modes over time and can be utilized to obtain best-fit linear models [40, 41, 48]. Identifying the nonlinear structure and parameters of dynamical models from data can be expensive due to the combinatorial possibilities for analyzing structures. Fortunately, the Sparse Identification of Nonlinear Dynamics (SINDy) algorithm provides a way to bypass costly searches by exploring the dependence of functional variables in the system [14]. On the other hand, Koopman operator theory presents an alternative perspective of dynamical systems in terms of the evolution of measurements because it is possible to represent a nonlinear dynamical system in terms of an infinite-dimensional linear operator acting on a Hilbert space of measurement functions of the state of the system [11, 16].

Machine learning (ML) and deep learning (DL) algorithms have emerged as powerful tools for modeling, predicting, and controlling dynamical systems, offering significant advantages over classical methods in handling nonlinearity, high dimensionality, and uncertainty. Recent advances in neural networks, Convolutional Neural Networks (CNN), and Recurrent Neural Networks (RNN) have demonstrated outstanding success in capturing temporal dependencies and chaotic behaviors in dynamical systems [13, 39]. Lusch et al. [30] used an autoencoder-based deep learning framework to discover Koopman eigenfunctions from data, enabling globally linear representations of nonlinear dynamics on low-dimensional manifolds. Moreover, [4] presented a Hopfield neural network-based method for online parameter estimation in system identification, featuring time-varying weights and biases to handle dynamic target functions. The simulations demonstrate better performance over classical gradient methods, achieving lower errors. A convolutional autoencoder and a multi-timescale recurrent neural network-based method are proposed in [43] for flexible behavior combination in robots using dynamical systems based on point attractors, incorporating instruction signals and phases to divide tasks into subtasks. Moreover, [47] proposed a feedforward network on a dynamical system's vector field using backpropagation, then converted it into a continuous-time RNN, demonstrating its effectiveness through numerical examples. Physics-informed neural networks (PINNs) have gained significant attention in recent years, [1] introduced Physics-Informed Neural Nets for Control, a novel framework extending traditional PINNs by incorporating initial conditions and control signals. It utilizes an autoregressive self-feedback method to provide accurate and adaptable simulations, as proven on nonlinear systems such as the Van der Pol oscillator with faster inference.

This paper presents a low-complexity structured neural network (StNN) designed to learn the dynamics of state-space systems and predict future states using a Hankel operator derived from a time-delay series of state measurements. We emphasize that Hankel matrices possess a unique structure, which can be effectively leveraged to solve systems of linear equations using low-complexity algorithms [5, 7, 22, 23, 33, 34]. Hankel matrices have been utilized in spectrum analysis, spectral decomposition, the evaluation of linear and chaotic stochastic dynamics, and the realization of state space systems [8, 26, 27, 32]. Furthermore, the modern Koopman operator theory

presents a compelling approach by employing delay embedding-based Hankel matrices as accurate computational tools for modeling dynamical systems, which is commonly known as delay-DMD or Hankel-DMD [2, 9, 48].

The paper is organized as follows. We propose a simple structured operator called the Hankel operator and utilize that to determine time advance states in dynamical systems using efficient computations in section 2. Next in Section section 3 we propose to optimize the operator to realize time-advanced states of dynamical systems. In Section 4, we introduce a StNN designed to effectively represent states in dynamical systems. This section details the network’s architecture, highlighting its advantages over conventional NN. Furthermore, we provide an analysis of the flop counts and parameter efficiency of our proposed network. In the following Section, section 5, we leverage the StNN to learn and update the states of the highly chaotic and extensively studied Lorenz system. This section will also showcase numerical results demonstrating the accuracy and precision of our proposed network. Additionally, we will conduct a long-term prediction analysis of our method, comparing its performance against conventional neural network predictions as well as those from SINDy and HAVOK, i.e., the delay-DM approach. Next, Section 5.1 presents results comparing StNN on an advanced approach for solving systems of ODEs across environments. Finally, we conclude the paper in section 6.

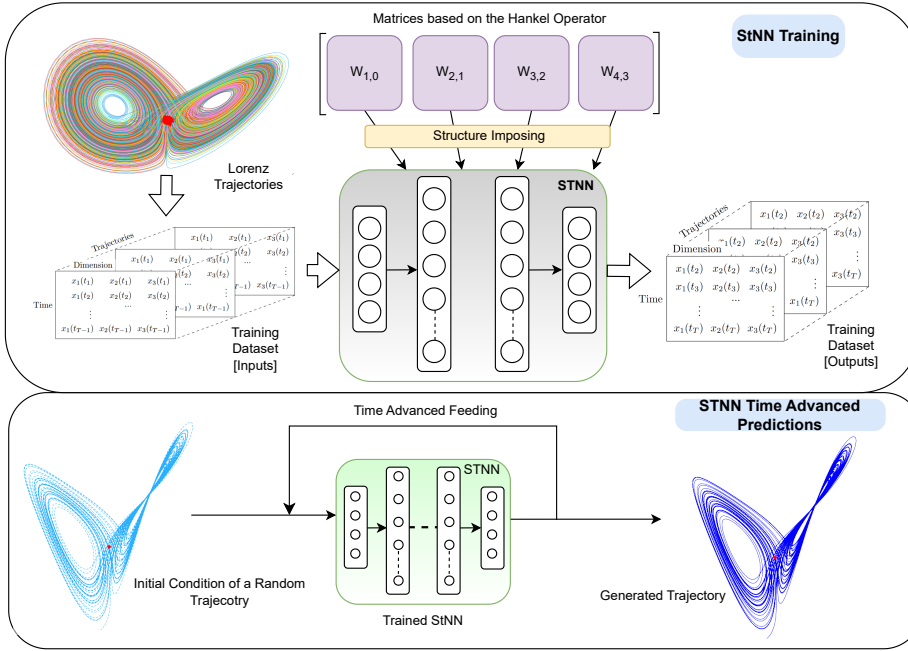


FIG. 1. An overview of the Structured Neural Network (StNN) framework for modeling dynamical systems. The top part depicts the StNN’s training process, which uses Lorenz system trajectories to create a dataset and structure-imposing matrices based on the Hankel operation to guide the learning process. The bottom portion shows time-advanced predictions, in which a trained StNN creates future trajectories based on an initial condition of a random trajectory

2. Preliminaries & Factorizations: Learning and Realizing States for Dynamical Systems. We propose to explore the chaotic behavior of dynamical systems by learning a real-valued Hankel structured operator. We note here that the structure-imposed operator is the key to proposing low-complexity learning. Thus, we will utilize data-driven learning to understand dynamical systems while proposing a low-complexity neural network called a StNN. Let us start the section by introducing notations which we will utilize frequently in the paper.

2.1. Frequently Used Notations. Here we introduce notations for sparse and orthogonal matrices which will frequently be used in this paper. We first define states of dynamical systems at time t_k by

$$(2.1) \quad \mathbf{x}_k = [x_1(t_k) \quad x_2(t_k) \quad \cdots \quad x_n(t_k)]^T,$$

where T for the transpose, and $k = 0, 1, \dots, n-1$. We utilize time-delays series of a state measurement $\{x(\tau_k)\}_{k=0}^{n-1}$ to define a Hankel operator \mathbf{H} s.t.

$$(2.2) \quad \mathbf{H} := \begin{bmatrix} x(\tau_0) & x(\tau_1) & x(\tau_2) & \cdots & x(\tau_{n-2}) & x(\tau_{n-1}) \\ x(\tau_1) & x(\tau_2) & x(\tau_3) & \cdots & x(\tau_{n-1}) & x(\tau_0) \\ x(\tau_2) & x(\tau_3) & x(\tau_4) & \cdots & x(\tau_0) & x(\tau_1) \\ \vdots & \vdots & \vdots & \vdots & \ddots & \vdots \\ x(\tau_{n-1}) & x(\tau_0) & x(\tau_1) & \cdots & x(\tau_{n-3}) & x(\tau_{n-2}) \end{bmatrix},$$

where τ_k 's are time-delay measurements. For a given vector $\mathbf{v} = [v_0, v_1, \dots, v_{n-1}]^T \in R^n$, let us introduce an even-odd permutation matrix \mathbf{P}_n ($n \geq 3$) by

$$\mathbf{P}_n \mathbf{v} = \begin{cases} [v_0, v_2, \dots, v_{n-2}, v_1, v_3, \dots, v_{n-1}]^T & \text{even } n, \\ [v_0, v_2, \dots, v_{N-1}, v_1, v_3, \dots, v_{n-2}]^T & \text{odd } n. \end{cases}$$

We also define the DFT matrix by $\mathfrak{F}_n = \frac{1}{\sqrt{n}} [w_n^{kl}]_{k,l=0}^{n-1}$, where $w_n = e^{-\frac{2\pi j}{n}}$ is the primitive n^{th} root of unity, a scaled DFT matrix by $\tilde{\mathfrak{F}}_n = \sqrt{n} \mathfrak{F}_n$ and its conjugate transpose by $\tilde{\mathfrak{F}}_n^*$, a highly sparse matrix by $\mathbf{J}_{r \times n} = \begin{bmatrix} \mathbf{I}_n \\ \mathbf{0}_n \end{bmatrix}$ where $r = 2n$, \mathbf{I}_n is the identity matrix and $\mathbf{0}_n$ is the zero matrix, an antidiagonal matrix by $\tilde{\mathbf{I}}_n$, a diagonal matrix by $\check{\mathbf{D}}_r = \text{diag} [\tilde{\mathfrak{F}}_r \mathbf{c}]$ where a circulant matrix \mathbf{C}_r defined by the first column

$$\mathbf{c} = [x(\tau_{n-1}), x(\tau_{n-2}), \dots, x(\tau_0), x(\tau_{n-1})],$$

\mathbf{c} s.t. $x(\tau_0), x(\tau_1), x(\tau_2), \dots, x(\tau_{n-2})]^T$.

2.2. Preliminaries: Dynamical Systems and Operator. This section introduces fundamentals related to dynamical systems derived from nonlinear ordinary differential equations (ODEs). We will also discuss an operator designed to effectively solve these dynamical systems. One could say that the nonlinear ODEs represent the dynamical system of the form

$$\frac{d}{dt} \mathbf{x}(t) = \mathbf{f}(\mathbf{x}(t), t),$$

where $\mathbf{x}(t) \in R^n$ is the state of the system evolving in time t and \mathbf{f} is a vector-valued function. As in the systems of linear equations, one could also answer the question of the existence and uniqueness of the dynamical systems. In this situation, this could

be generally achieved by analyzing the Lipschitz continuity of the function \mathbf{f} . On the other hand, the discrete-time dynamical systems are of the form

$$\mathbf{x}_{k+1} = \mathbf{F}(\mathbf{x}_k),$$

and it sees the states of the system at the k^{th} iteration as $\mathbf{x}_k \in \mathbb{R}^n$ having a non-linear function \mathbf{F} , which will usually denote iterations forward in time, so that $\mathbf{x}_k = \mathbf{x}(k\Delta t)$. This is the situation, in which we could seek the solution of a dynamical system as a solution of a system of linear equations. Thus, to sum up, many problems in dynamical systems ultimately lead to a solution of systems of linear equations. On the other hand and due to the nonlinear nature of these dynamical systems, we propose a learning algorithm to train a neural network so that the network could learn an updated state from \mathbf{x}_k (2.1) to \mathbf{x}_{k+1} using a low-complexity ML operator. To learn an operator, we start with a vector-valued measurement function $g : M \rightarrow \mathbb{R}^n$ which are elements of an infinite-dimensional Hilbert space, i.e., Lebesgue square-integrable functions on a smooth manifold M . We define so-called a Hankel operator \mathbf{H} (2.2) via time-delays series of a state measurement $\{x(\tau_k)\}_{k=0}^{n-1}$ and extend it to states \mathbf{x}_k by using time snapshots of spatiotemporal data that act on the measurement functions g s.t. $\mathbf{H}g(\mathbf{x}) = (g \circ \mathbf{F})(\mathbf{x})$, where \circ is the composition operator and \mathbf{F} is the non-linear function. More precisely for the discrete-time system with time-step $\Delta\tau$, the Hankel operator is defined as

$$(2.3) \quad \mathbf{H}g(\mathbf{x}_k) = g(\mathbf{F}(\mathbf{x}_k)) = g(\mathbf{x}_{k+1}).$$

In other words, the proposed Hankel operator defines linear dynamical systems that advance the observations of the state \mathbf{x}_k , i.e., $g_k = g(\mathbf{x}_k)$ to the next time-advanced observations g_{k+1} s.t.

$$g(\mathbf{x}_{k+1}) = \mathbf{H}g(\mathbf{x}_k),$$

for $k = 0, 1, \dots, n - 1$. We note that the Hankel operator is linear in the function spaces s.t. $\mathbf{H}(c_1g_1(\mathbf{x}) + c_2g_2(\mathbf{x})) = c_1\mathbf{H}g_1(\mathbf{x}) + c_2\mathbf{H}g_2(\mathbf{x})$, where c_1 and c_2 are constants and g_1 and g_2 are measurement functions.

Finally, we note that the Hankel operator for the dynamical systems evolved with continuous- time is defined as

$$\frac{d}{dt}g(\mathbf{x}) = \mathbf{H}g(\mathbf{x}).$$

Thus, having a rich set of information based on the time-delayed operator \mathbf{H} to predict future states of chaotic systems leads to better prediction than linear or nonlinear systems with trajectories trapped at fixed points or on periodic orbits [12]. On the other hand, instead of advancing linear or non-linear measurements of the states of a system, like in the DMD, we could measure time-delayed measurements using the Hankel operator \mathbf{H} following the HAVOK [2, 10] and utilize that to obtain low-complexity algorithms to realize state measurements.

2.3. Factorize the Hankel Operator to Realize State Measurements.

In this section, we propose to utilize the factorization of the Hankel operator to realize state measurements using low-complexity algorithms. This is due to the fact that the data-driven approaches are computationally intensive, despite the potential for low-rank approximation via established SVD techniques. However, Hankel is a

structured matrix, which allows us to explore an alternative approach for low-rank approximation in HAVOK. Instead of depending on SVD, we propose utilizing low-complexity algorithms that leverage the inherent structure of the Hankel operator to observe time-advanced states. This approach aims to reduce the complexity of training data-driven models efficiently.

PROPOSITION 2.1. *Let \mathbf{H} be the Hankel operator (2.2) determined via time-delays series of a state measurement $\{x(\tau_k)\}_{k=0}^{n-1}$. Then, the Hankel operator can be utilized to advance the state \mathbf{x}_k to the next time-advanced state \mathbf{x}_{k+1} through the summation of the following low-rank matrices*

$$(2.4) \quad \begin{aligned} \mathbf{x}_{k+1} &= \mathbf{H}\mathbf{x}_k \\ &= \mathbf{J}^T [x_1(t_k)\tilde{\mathbf{x}} + x_2(t_k)\mathbf{Z}\tilde{\mathbf{x}} + x_3(t_k)\mathbf{Z}^2\tilde{\mathbf{x}} + \cdots + x_n(t_k)\mathbf{Z}^{n-1}\tilde{\mathbf{x}}], \end{aligned}$$

where \mathbf{Z} is $r \times r$ upper shift matrix and

$$\tilde{\mathbf{x}}_{r \times 1} = [x(\tau_0), x(\tau_1), x(\tau_2), \cdots, x(\tau_{n-1}), x(\tau_0), x(\tau_1), \cdots, x(\tau_{n-2}), 0]^T.$$

Proof. The operator \mathbf{H} is a symmetric Hankel matrix determined by the first column(or row) of \mathbf{H} s.t. $[x(\tau_0), x(\tau_1), \cdots, x(\tau_{n-1})]^T$, and when Z is the lower shift matrix and when $\tilde{\mathbf{x}}_{r \times 1}$ is defined as above, we could write $\mathbf{H} = [\tilde{\mathbf{x}}, Z\tilde{\mathbf{x}}, \cdots, Z^{n-1}\tilde{\mathbf{x}}]$. Thus by taking $\mathbf{H}\mathbf{x}_k$ as a linear combination of the columns of \mathbf{H} with scaling factors corresponding to the state \mathbf{x}_k followed by scaling \mathbf{J}^T and equation (2.3), we could compute $\mathbf{H}\mathbf{x}_k$ to realize \mathbf{x}_{k+1} via (2.4). \square

COROLLARY 2.2. *Let the Hankel operator \mathbf{H} be utilized to advance the observation of states from \mathbf{x}_k to \mathbf{x}_{k+1} using Proposition 2.1, then complexity in realizing time-advanced states cost $\mathcal{O}(n^s)$, where $1 < s < 2$.*

Proof. Since \mathbf{H} is the structured matrix determined by $\mathcal{O}(n)$ elements, we could compute $\mathbf{H}\mathbf{x}_k$ by utilizing the upper shift matrix $\mathbf{Z}_{r \times r}$ followed by the vector $\tilde{\mathbf{x}}_{r \times 1}$ in (2.4) to reduce the complexity in computing the conventional matrix-vector product of $\mathbf{H}\mathbf{x}_k$ from $\mathcal{O}(n^2)$ to $\mathcal{O}(n^s)$, where $1 < s < 2$. \square

By utilizing the radix-2 algorithm to compute the Toeplitz matrices by a vector using 2-FFTs [6, 37] as opposed to 3-FFTs [28, 36] for an even length s.t. $n = 2^p (p \geq 1)$, and also computing the odd order Toeplitz matrices by a vector using 2-FFTs in [35], we could also state the following factorization to decompose the Hankel operator \mathbf{H} using 2-FFTs.

PROPOSITION 2.3. *Let \mathbf{H} be the Hankel operator (2.2) determined via time-delays series of a state measurement $\{x(\tau_k)\}_{k=0}^{n-1}$. Then, the time-advanced states \mathbf{x}_{k+1} can be computed using the time-delayed states \mathbf{x}_k followed by the decomposition of \mathbf{H} s.t.*

$$(2.5) \quad \mathbf{x}_{k+1} = \mathbf{H}\mathbf{x}_k = \tilde{\mathbf{I}}_n \hat{\mathbf{D}}_n [\mathbf{J}^T]_{n \times r} \mathbf{C}_r [\mathbf{J}]_{r \times n} \hat{\mathbf{D}}_n \cdot \mathbf{x}_k,$$

where the circulant matrix $\mathbf{C}_r = \check{\mathfrak{F}}_r^* \check{\mathbf{D}}_r \check{\mathfrak{F}}_r$, and $\hat{\mathbf{D}}_n = \left[\text{diag}(e^{-\frac{\pi k^2 i}{n}}) \right]_{k=0}^{n-1}$.

Proof. When $n = 2^p (p \geq 1)$, we could compute $\mathbf{H}\mathbf{x}_k$ by using the 2-FFTs as described in [37], and when $n \neq 2^p$, we could again compute $\mathbf{H}\mathbf{x}_k$ by using the 2-FFTs in [35]. \square

COROLLARY 2.4. *Let the Hankel operator \mathbf{H} be utilized to advance the observation of states from \mathbf{x}_k to \mathbf{x}_{k+1} using Proposition 2.3, then complexity in realizing time-advanced states is $\mathcal{O}(n \log n)$.*

Proof. As for any n , the product $\mathbf{H}\mathbf{x}_k$ could be computed using the 2-FFTs [35, 37], and hence the complexity in computing $\mathbf{H}\mathbf{x}_k$ to realize time advanced states cost $\mathcal{O}(n \log n)$. \square

3. A Best-fit Operator to Advance States. Following the previous section, we propose to obtain a best-fit operator for the Hankel operator \mathbf{H} —say $\widehat{\mathbf{H}}$ (w.l.o.g. let us assume that $m \geq n$), determined via time snapshots of spatiotemporal data. Furthermore, we propose to enhance learning by capturing the evolution of the nonlinear dynamical system using data-driven embedding based on an optimized operator.

3.1. Learn a Best-fit Operator. We first obtain a best-fit operator—say $\widehat{\mathbf{H}}$ determined via time-delays series of a state measurement $\{x(\tau_k)\}_{k=0}^{n-1}$ to optimize the data-driven learning.

PROPOSITION 3.1. *Let $\mathbf{X}_{l,k} = [x_l(\tau_k)]_{l=1,k=0}^{n,n-1}$ is the time-delay snapshots matrix, $\mathbf{X}'_{l,k} = [x_l(t_k)]_{l=1,k=0}^{n,n-1}$ is the time-advanced snapshots matrix, $t_k = \tau_k + \Delta t$, and Δt is the timestep. Then, an approximate solution for the Hankel operator \mathbf{H} —say $\widehat{\mathbf{H}}$ can be obtained via*

$$(3.1) \quad \mathbf{X}' \approx \widehat{\mathbf{H}}\mathbf{X}, \quad \widehat{\mathbf{H}} = \operatorname{argmin}_{\mathbf{H}} \left\{ \frac{1}{2} \|\mathbf{X}' - \mathbf{H}\mathbf{X}\|_F^2 + \alpha \|\mathbf{H}\|_\eta \right\},$$

where $\|\cdot\|_F$ is the Frobenius norm, $\|\cdot\|_\eta$ represents the nuclear norm for low-rank matrices, and α is a non-negative tuning parameter controlling the regularization of the low-rank matrix.

Proof. Without loss of generality, we consider \mathbf{H}^T : the transpose of the Hankel operator \mathbf{H} since the singular values of the \mathbf{H}^T are equal to those of \mathbf{H} . Now (3.1) is equivalent to the following formulation

$$(3.2) \quad (\mathbf{X}')^T \approx \mathbf{X}^T \widehat{\mathbf{H}}^T \quad \text{where, } \widehat{\mathbf{H}}^T = \operatorname{argmin}_{\mathbf{H}^T} \left\{ \frac{1}{2} \|(\mathbf{X}')^T - \mathbf{X}^T \mathbf{H}^T\|_F^2 + \alpha \|\mathbf{H}^T\|_\eta \right\},$$

which is a convex optimization problem due to the fact that the nuclear norm $\|\cdot\|_\eta$ is a convex relaxation of the rank minimization problem [45]. Moreover, because this norm is coercive, there exists an optimal solution for (3.2). By the framework in [25], the formulated optimization problem (3.2) can be solved equivalently as

$$(3.3) \quad \widehat{\mathbf{H}}^T = \operatorname{argmin}_{\mathbf{H}^T} \left\{ \|\mathbf{H}^T - \left(\mathbf{H}_{k-1}^T - \frac{1}{t_k} \mathbf{X}(\mathbf{X}^T \mathbf{H}_{k-1}^T - (\mathbf{X}')^T) \right)\|_F^2 + \frac{2\alpha}{t_k} \|\mathbf{H}^T\|_\eta \right\},$$

where \mathbf{H}_{k-1}^T is the $k-1$ iterates for H and t_k is the stepsize. The minimization problem (3.3) can be solved by computing the singular value decomposition (SVD) of $\left(\mathbf{H}_{k-1}^T - \frac{1}{t_k} \mathbf{X}(\mathbf{X}^T \mathbf{H}_{k-1}^T - (\mathbf{X}')^T) \right)$. Then the soft-thresholding operator can be applied on the singular values. By Theorem 2.1 in [15], the approximate solution for (3.3) has low-rank properties, which can be chosen as an approximate solution for the Hankel operator. \square

Once the data-driven dynamical system has evolved, it is possible to further enhance the algorithms to differentiate between the inherent, spontaneous dynamics and the impact of actuation. This differentiation amounts to a more comprehensive evolution equation [38]

$$(3.4) \quad \mathbf{x}_{k+1} \approx \widehat{\mathbf{H}}\mathbf{x}_k + \mathbf{G}\mathbf{u}_k,$$

where $\widehat{\mathbf{H}}$ is an $n \times n$ system matrix realized as the best-fit Hankel operator, \mathbf{G} is an $n \times q$ input matrix and $\mathbf{u}_k = [u_1(t_k) \ u_2(t_k) \ \cdots \ u_q(t_k)]^T \in \mathbb{R}^q$ is an input vector. The system extension (3.4) stems from (3.1) leads to seek time-advanced states using time-delayed states-based Hankel operator.

4. A Structured Neural Network (StNN) for Dynamical Systems. We show in this section that the Hankel operator can effectively predict time-advanced trajectories of dynamical systems using a low-complexity neural network, following the efficient learning and updating of the system's dynamics. Thus, we introduce the StNN, showing its efficiency in training, learning, and updating dynamical systems, especially when compared with conventional feedforward neural networks. The StNN layers are designed using the matrix factorization of the Hankel operator (2.2), which imposes significant constraints that minimize complexity and enhance performance. We begin with an overview of the StNN's construction, followed by its layer architecture, based on the matrix factorization of the Hankel operator (2.5). Simply, we introduce an integration of model-based and data-driven learning with the design of StNN. The Figure 1 illustrates the training and prediction process of the StNN for modeling the Lorenz system. The upper section represents the StNN Training phase, where Lorenz trajectories are used to generate a training dataset comprising input and output sequences. The StNN is trained to map past trajectory points to future states, learning the underlying dynamics of the system. The lower section depicts the StNN autoregressive predictions phase, where a trained StNN takes the initial condition of a random trajectory as input and iteratively predicts future states. This process results in a generated trajectory that closely follows the true Lorenz dynamics. The structured approach enhances the model's ability to capture chaotic behavior.

4.1. Structured Neural Network Architecture. We start the section with the forward propagation of the StNN followed by its architecture. The forward propagation of the StNN leverages the factorization equation (2.5) through specialized layers that incorporate diagonal matrices and recursive operations derived from the factorization of the Hankel operator. This approach is complemented by a layer-by-layer computation process utilizing matrix-vector products, which enables the StNN to achieve enhanced states effectively.

PROPOSITION 4.1. *Let $\mathbf{x}_0 \in \mathbb{R}^{m \times 1}$ be the input vector, $\mathbf{x}_4 \in \mathbb{R}^{m \times 1}$ be the output vector, and m be the number of nodes in each layer of a neural network. Let the output between the $(i-1)$ -th and i -th hidden layer be given by:*

$$(4.1) \quad \mathbf{x}_i = \sigma_i(W_{i,i-1}\mathbf{x}_{i-1} + \mathbf{b}_i)$$

where $i := \{1, 2, 3, 4\}$, $W_{i,i-1}$ is the weight matrix connecting the $(i-1)$ -th layer to the i -th layer, \mathbf{b} represents the bias vector, and σ is the activation function. Then, we can design a StNN to predict states \mathbf{x}_{k+1} from \mathbf{x}_k using the weight matrices defined via $W_{1,0} \in \mathbb{R}^{2pm \times m}$, $W_{2,1} \in \mathbb{R}^{pm \times 2pm}$, $W_{3,2} \in \mathbb{R}^{pm \times pm}$, $W_{4,3} \in \mathbb{R}^{m \times pm}$, and their p number of parallel sub-weight matrices, denoted as $w_{i,i-1}$, with the following structured weight matrices

$$W_{1,0} = \begin{bmatrix} w_{1,0} \\ w_{1,0} \\ \vdots \\ w_{1,0} \end{bmatrix}_{2pm \times m}, \quad W_{2,1} = \begin{bmatrix} w_{2,1} & 0 & \dots & 0 \\ 0 & w_{2,1} & \dots & 0 \\ \vdots & \vdots & & \vdots \\ 0 & 0 & \dots & w_{2,1} \end{bmatrix}_{pm \times 2pm},$$

$$W_{3,2} = \begin{bmatrix} w_{3,2} & 0 & \dots & 0 \\ 0 & w_{3,2} & \dots & 0 \\ \vdots & \vdots & & \vdots \\ 0 & 0 & \dots & w_{3,2} \end{bmatrix}_{pm \times pm}, \quad W_{4,3} = [w_{4,3} \quad w_{4,3} \quad \dots \quad w_{4,3}]_{m \times pm},$$

where $w_{1,0} = \mathfrak{F}_{2m}^*[J]_{2m \times m} \hat{D}_m \in \mathbb{R}^{2m \times m}$, $w_{2,1} = [J^T]_{m \times 2m} \mathfrak{F}_{2m} \check{D}_{2m} \in \mathbb{R}^{m \times 2m}$, $w_{3,2} = \tilde{\mathbf{I}}_m \hat{D}_m \in \mathbb{R}^{m \times m}$, and $w_{4,3} = D_m \in \mathbb{R}^{m \times m}$.

Proof. Let us define the sub-matrices $w_{1,0} \in \mathbb{R}^{2m \times m}$, $w_{2,1} \in \mathbb{R}^{m \times 2m}$, $w_{3,2} \in \mathbb{R}^{m \times m}$, and $w_{4,3} \in \mathbb{R}^{m \times m}$ based on the factorization of the Hankel operator (2.5) to design layers and learn weights for the proposed network. We begin by grouping the matrices in the factorization (2.5) into three distinct groups, ensuring each group corresponds to the weight matrices connecting $(i-1)$ -th layer to the i -th layer. In the first hidden layer, we define j parallel sub-weight matrices s.t. $w_{1,0} = \mathfrak{F}_{2m}^*[J]_{2m \times m} \hat{D}_m$, to learn the weight matrix $W_{1,0}$. Next, the sub-weight matrices connecting the first and second hidden layers are defined by $w_{2,1} = [J^T]_{m \times 2m} \mathfrak{F}_{2m} \check{D}_{2m}$ which are utilized to learn the weight matrix $W_{2,1}$. Next, the sub-weight matrices between the second and third hidden layers are defined as $w_{3,2} = \tilde{\mathbf{I}}_m \hat{D}_m$, and we utilize those to learn the weight matrix $W_{3,2}$. After the third hidden layer, the sub-weight matrices connecting the last hidden layer to the output layer are represented as diagonal matrices, i.e., $w_{4,3} = D_m$. Consequently, a linear transformation is applied to combine the outputs of the sub-weight matrices to learn the weight matrix $W_{4,3}$. In addition to these weight matrices, we have frozen all identity and zero matrices in the factorization of the Hankel operator (2.5) at each network layer. This will enable us to develop a lightweight model. Also, we have not shared or reused matrices among different layers, ensuring that no additional matrices contribute to the network architecture. With this configuration of parallel sub-weight matrices and frozen matrices, along with the propagation described in equation (4.1), we efficiently train the weight matrices of the StNN using a lightweight model. \square

To illustrate the advantages of our proposed network architecture over the feed-forward neural network (FFNN), we will present the structure of the StNN alongside the FFNN followed by the flop count, as detailed in Table 1.

4.2. Structured Neural Network Approach to Predict Trajectories of Dynamical Systems. To study the evolution of the dynamical system, we first focus on the simple Lotka-Volterra model, followed by the well-studied and highly chaotic Lorenz system. We compare StNN and LEADS for the Lotka-Volterra model and StNN, FFNN, SINDy, and HAVOK for the Lorenz system. Our goal is to compare their accuracy, flop counts, parameters, and long-term behavior to efficiently predict the time-advanced trajectories of the system.

The Lotka-Volterra model is defined via a set of nonlinear ODEs known as a

TABLE 1

The StNN and FFNN architectures are designed for the layer-wise comparison of weight matrices, biases, total number of parameters, and flop counts. The value p denotes the number of parallel sub-weight matrices designed for the values $p = 1, 2, 4, 6$, which correspond to four distinct StNN models. These sub-matrices are used to construct and learn weight matrices $W_{i,i-1}$ that connect the $(i-1)$ -th layer to the i -th layer for $i = 1, 2, 3, 4$.

Weight Matrix	Sub Weight Matrices	Number of Parallel Sub Weight Matrices	Weights	Biases	Total Parameters	flop Count
StNN (Structured Neural Network)						
$W_{1,0}$	$[\hat{\mathbf{D}}]_{4 \times 4}$	p	$4p$			
	$[\hat{\mathcal{S}}_2]_{2 \times 2}$	$2p$	$8p$	$8p$	$26p$	$68p$
	$[\mathbf{H}]_{8 \times 8}$	p	$4p$			
	$[\mathbf{H}]_{4 \times 4}$	p	$2p$			
	Total	-	18p	8p	26p	68p
$W_{2,1}$	$[\hat{\mathbf{D}}]_{8 \times 8}$	p	$8p$			
	$[\hat{\mathcal{S}}_2]_{2 \times 2}$	$2p$	$8p$	$4p$	$26p$	$68p$
	$[\mathbf{H}]_{8 \times 8}$	p	$4p$			
	$[\mathbf{H}]_{4 \times 4}$	p	$2p$			
	Total	-	22p	4p	26p	68p
$W_{3,2}$	$[\hat{\mathbf{D}}]_{4 \times 4}$	p	$4p$	$4p$	$8p$	$8p$
$W_{4,3}$	$[\hat{\mathbf{D}}]_{4 \times 4}$	p	$4p$	$4p$	$8p$	$12p - 4$
Total	-	-	48p	20p	68p	156p - 4
FFNN (Feed-forward Neural Network)						
$W_{1,0}$	$[W]_{30 \times 3}$	-	90	30	120	180
$W_{2,1}$	$[W]_{30 \times 30}$	-	900	30	930	1800
$W_{3,2}$	$[W]_{30 \times 30}$	-	900	30	930	1800
$W_{4,3}$	$[W]_{3 \times 30}$	-	90	3	93	180
Total	-	-	1980	93	2073	3960

"predator-prey" system and formulated as

$$\frac{dx}{dt} = \alpha x - \beta xy, \quad \frac{dy}{dt} = -\gamma y + \delta xy,$$

where $\alpha, \beta, \gamma, \delta$ are system parameters which define an *environment* and x and y respectively represent prey and predator populations.

On the other hand, the Lorenz system is determined via a system of differential equations in the form

$$(4.2) \quad \frac{dx}{dt} = \sigma(y - x), \quad \frac{dy}{dt} = x(\rho - z) - y, \quad \frac{dz}{dt} = xy - \beta z$$

where the state of the system is given by $\mathbf{x} = [x, y, z]^T$ with the parameters $\sigma = 10, \rho = 28$, and $\beta = 8/3$. Thus, before starting the numerical simulations based on the StNN to solve the Lotka-Volterra model and predict time-advanced trajectories of the Lorenz system, we will cover the fundamentals of the proposed StNN.

To obtain the evolution of the Lorenz system, we generate a wide range of initial conditions, denoted by vector \mathbf{x}_0 , and track the trajectories over time. We advance the initial conditions with a sampling time interval of Δt , which is not the actual time step. The next step is to acquire the matrices that represent the inputs and outputs of the system at states \mathbf{x}_k and \mathbf{x}_{k+1} , respectively, with sample increments of Δt , which are correlated to \mathbf{X} and \mathbf{X}' , respectively. These matrices are obtained by utilizing the trajectories that have been trained over time through the learned Hankel operator \mathbf{H} . Thus to capture the evolution of the non-linear nature of the dynamical systems, we

use StNN and FFNN with 5 layers (when including the input, output, and 3 hidden layers) and different number of nodes in each layer while imposing the structure to the network using Propositions 2.3 and 4.1, in order to carry on the forward propagation. The network will be trained on trajectories based on (3.4) to predict states in future time for any given initial conditions. The network will utilize activation functions such as Tanh and Sigmoid in the first two hidden layers and ReLU as the activation function of the third hidden layer to incorporate the dynamics of the system. As a result, we derive a new set of spatiotemporal data to generate future predictions from \mathbf{x}_k to \mathbf{x}_{k+1} .

Additionally, we evaluate the training performance over e epochs, using the loss function based on Proposition 3.1 s.t.

$$L(\mathbf{x}_k, \mathbf{x}_{k+1}) := \|\mathbf{X}' - \widehat{\mathbf{H}}\mathbf{X}\|^2,$$

and hence validate the trajectory data of the trained model against the dynamical model using the best-fit time advanced state-based Hankel operator $\widehat{\mathbf{H}}$.

5. Numerical Simulations: Learn, Update, and Predict States. In this section, we first learn, update, and predict trajectories for the Lotka-Volterra model followed by the chaotic Lorenz system. Next, we compare numerical simulations based on the StNN and LEADS for the Lotka-Volterra model and StNN, FFNN, SINDy, and HAVOK for the Lorenz system.

5.1. Numerical Simulations: Lotka-Volterra Model to Learn and Predict Dynamics. In this section, we show numerical simulations to determine the time evolution of the Lotka-Volterra model for different *environments*, where each environment is described by a set of system parameters α, β, γ , and δ . In this experiment, we also draw comparisons with recently proposed model for dynamical systems, LEADS [49]. LEADS is a framework that leverages the commonalities and discrepancies among known environments to improve model generalization, using separate model components that focus either on global or environmental-specific dynamics. Following the experimental setup from LEADS, we consider 10 possible environments and generate trajectories each with 20 data points in time, $t_k = 0.0, 0.5, 1.0, \dots, 9.5$. For training, we sample 8 trajectories from each environment. Each environment has a unique set of system parameters, while each trajectory has a unique set of initial conditions. At evaluation, the models are tested on 32 trajectories from each environment. The model receives $x(t_k), y(t_k), t_k$ and the *environment* passed as a unique integer which parametrizes the system parameters. The goal is to predict $x(t_{k+1}), y(t_{k+1})$ as outputs of the model. During the evaluation, the model only receives the initial conditions $x(t_0), y(t_0), t_0 = 0$, and environment specifier, performing an autoregressive rollout to predict all future x, y . The results of this experiment are summarized in Table 2 and examples of predictions are provided in Figure 2.

TABLE 2

Test results of the StNN on the Lotka-Volterra equations. Baseline experiments with the LEADS model [49] show that the proposed approach is able to obtain remarkable accuracy with very few parameters.

Model	Training Time	Parameters	MSE
StNN	53 s	388	$(2.02 \pm 0.39) \times 10^{-3}$
LEADS	615 s	95095	$(3.17 \pm 2.41) \times 10^{-3}$

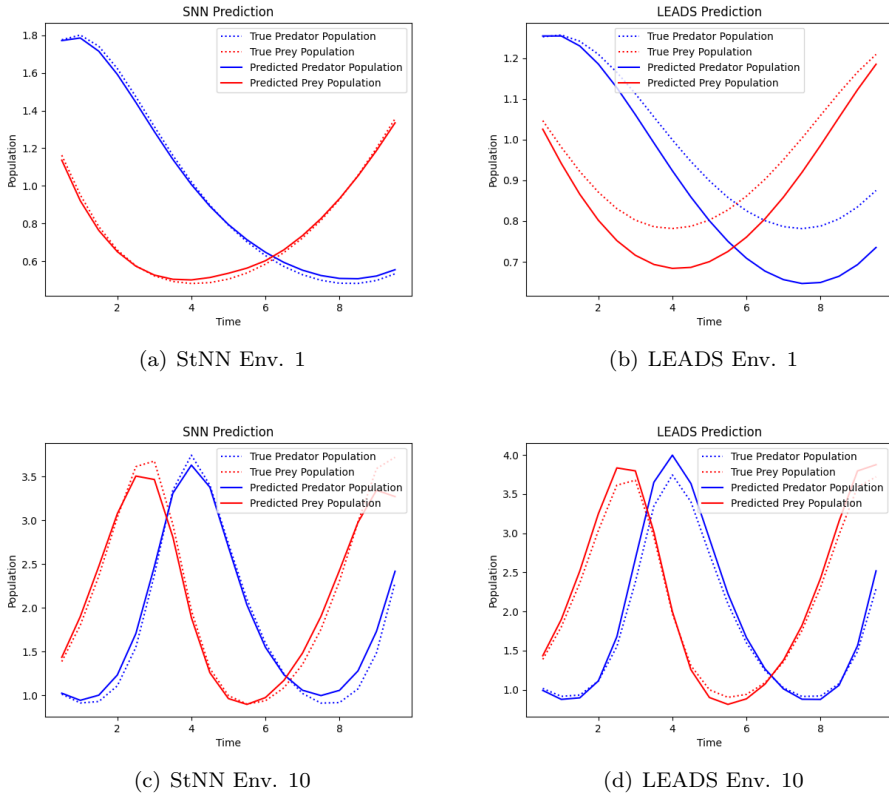


FIG. 2. Autoregressive rollouts over 20-time steps of the respective models for the Lotka-Volterra system. While LEADS shows some divergence with the true solution at later times, StNN remains close to the true solution.

Although LEADS was designed with novel elements to improve generalization across environments, we observe that large deviations from the truth may arise in some instances, illustrated in Figure 2 (b). Meanwhile, StNN predicts dynamics which remain close to the ground truth. Additionally, Table 2 illustrates several advantages of the StNN in parameter complexity and training time requirements. While LEADS has nearly 100,000 parameters, StNN is able to achieve a competitive error with a remarkable 388 trainable parameters. As a result, StNN may also be trained an entire order of magnitude faster than the competing approach. This experiment underlines the advantages of structured matrices with learnable parameters, as we propose in this work.

5.2. Numerical Setup for the Chaotic Lorenz System. In this section, we analyze the performance of the StNN architecture compared to FFNN, SINDy, and HAVOK using the chaotic Lorenz system. To conduct these simulations, the Lorenz system, characterized by the differential equations (4.2), was used to produce time-series data based on the parameters $\sigma = 10$, $\beta = \frac{8}{3}$, and $\rho = 28$ with a time step of $dt = 0.01$ at the duration of $T = 8$, i.e. each trajectory consists of 800 data points. Furthermore, we obtained 100 such trajectories by perturbing the nominal initial state, i.e. $[x(t_0), y(t_0), z(t_0)] = [0, 1, 20]$ with random uniform noise of magnitude 1.

The `odeint` function from the SciPy library was used to numerically integrate each perturbed trajectory, guaranteeing high accuracy with relative and absolute tolerances set to 1×10^{-12} . Figure 3 shows the trajectories of the Lorenz attractor, along with 100 randomly perturbed trajectories originating from the initial states, represented by red dots.

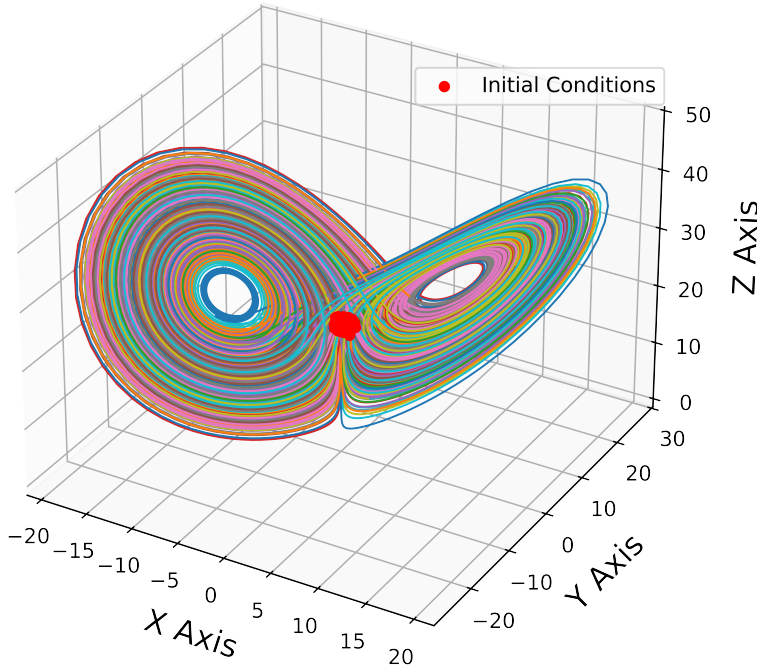
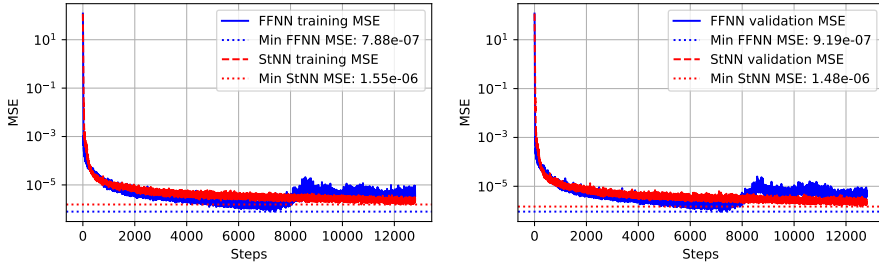


FIG. 3. Visualization of Lorenz system trajectories with random perturbations in initial conditions. The red dots represent the perturbed starting points, and the lines illustrate the chaotic evolution of the system.

As shown in Figure 4, we observed that the trained StNN reproduced the chaotic dynamics of the system with high accuracy and reduced complexity as compared to the FFNN. This is evident from the training and validation MSE comparison between the StNN and the FFNN in Figure 4. The SNN maintains a more resource-efficient architecture while demonstrating a smoother training MSE curve, which shows steady performance gains over time. This demonstrates how the chosen StNN can balance computational efficiency and accuracy, making it a competitive alternative to the FFNN. However, the FFNN, having a larger number of trainable weights, demonstrates greater flexibility and achieves lower MSE rates. The reason is that the increased capacity of the FFNN allows it to better approximate the target function. Conversely, StNN’s reduced parameterization naturally imposes constraints on the network’s flexibility, resulting in a slightly higher overall MSE. Despite this, the StNN’s lightweight architecture offers significant advantages in terms of computational efficiency, making it an appealing choice for scenarios where inference speed and resource constraints are critical considerations.

5.3. Numerical Simulations of NNs: Learn and Update. The StNN was implemented using a feedforward architecture with input, output, and three hidden



(a) FFNN and StNN training MSE over steps (b) FFNN and StNN validation MSE over steps

FIG. 4. *Training and validation MSE comparison for FFNN and StNN models over states evaluated at time steps. Each step represents a randomly sampled mini-batch from the dataset, with 640 steps:= 1 training epoch. The plots illustrate the convergence behavior, showing how the MSE evolves as training progresses. The plot (a) depicts training MSE, while the plot (b) shows validation MSE. While the FFNN (blue) shows a lower minimum MSE than the StNN (red) during both training and validation, The dotted lines represent the minimum recorded MSE for each model. Moreover, Table 3 illustrates that the StNN is more lightweight than the FFNN, resulting in reduced complexity.*

layers, as explained in Section 4.2. This model effectively combines activation functions (tanh, *Sigmoid*, and *ReLU*) to capture the complex non-linear dynamics of the Lorenz system. The input and output dimensions were set to 4 by padding the state variables (x, y, z) with 0, i.e., $(x, y, z, 0)$ to match the dimensions.

An 80,000-sized randomly generated dataset was divided into input-output pairs, with each input being a state vector $[x_1(t_k), x_2(t_k), x_3(t_k), 0]$ and the output being the subsequent state vector $[x_1(t_{k+1}), x_2(t_{k+1}), x_3(t_{k+1}), 0]$. The input and output datasets were mini-batched 1000 to ensure efficient mini-batch-wise training[21] We split the dataset into training and validation, i.e., 80% of the dataset was allocated for training, while the remaining 20% was reserved for validation. To enhance readers' understanding of the theoretical foundation and its connection to the StNN learning algorithm, we direct readers to the code [StNN-Dynamical-Systems](#).

We utilized the Levenberg-Marquardt algorithm implemented in PyTorch by Di Marco [31]. This implementation enables efficient optimization for training neural networks by combining the advantages of gradient descent and Newton's method. The training process was conducted over 20 epochs with 640 steps for each epoch, utilizing the high convergence rate of the Levenberg-Marquardt method for non-linear regression tasks. First, we present the convergence performance of the StNN in comparison with the FFNN while varying the number of sub-weight matrices p . As discussed in Section 4, the StNN can be represented using multiple parallel sub weight matrices, denoted as p . The selection of an appropriate value for p should be guided by the desired MSE and the specific complexity requirements of the system. A summary of the training and validation performance for various StNN models with different p values is provided in Table 3. The flop savings percentages are calculated in comparison to the FFNN using

$$(5.1) \quad \text{Saving\%} = \frac{\#\text{FFNN}(\text{count}) - \#\text{StNN}(\text{count})}{\#\text{FFNN}(\text{count})} \times 100\%.$$

Smaller p values lead to higher MSEs, reflecting the trade-off between model simplicity and accuracy. While smaller p values reduce the number of weights and

TABLE 3

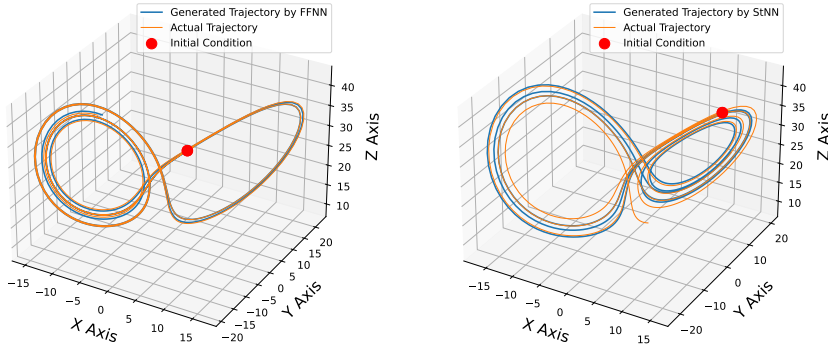
We show the training and validation performance of StNN for different numbers of parallel p sub-weight matrix configurations. This table summarizes the impact of varying p on Mean Squared Error (MSE), model weights, and computational complexity (flops). Savings percentages are calculated in comparison to the FFNN using equation (5.1).

p	Final Training MSE	Parameter Saving compared to FFNN in Table 1	flop Saving compared to FFNN in Table 1
1	1.49×10^{-4}	96%	96%
2	2.47×10^{-4}	94%	92%
4	2.67×10^{-6}	87%	84%
6	5.26×10^{-6}	81%	76%

floating-point operations, they also result in less precise predictions over time. Conversely, larger p values yield significantly lower MSEs, highlighting their excellent predictive accuracy. However, this improvement comes at the cost of increased computational complexity, as seen in the greater number of weights and flops required. Interestingly, when compared to other StNN configurations, the best-performing StNN model is $p = 6$, which achieves a significant reduction in the error on the dataset. Furthermore, compared to the FFNN, this StNN achieves a reduction of roughly 81% in the number of weights and 76% in floating-point operations, demonstrating a significant advantage in computational and parameter complexity.

5.4. Numerical Simulations of NNs: Time Evolution. Once the StNN and FFNN are trained and updated on the trajectory data in Section 5.3, the non-linear dynamical model describing the Lorenz system could be to map the states from \mathbf{x}_k to \mathbf{x}_{k+1} and hence to predict the future states from an initial state. Figure 5 was created using the trained StNN and FFNN to take an initial state and autoregressively advance the solution by Δt . The output at each time stamp was reinserted into the NNs to estimate the solution $k\Delta t$ to predict time-advanced states. This iterative mapping could produce a prediction for the future state as far into the future as desired. More specifically, figure 5 shows states mapping from \mathbf{x}_k to \mathbf{x}_{k+1} to predict Lorenz solution 600-time steps into the future from a given initial state. The performance of the StNN was then compared with the FFNN to approximate the future dynamics of the system. The evolution of two randomly chosen trajectories is predicted using the StNN and FFNN as shown in figure 5. Both networks show remarkable accuracy in predicting highly chaotic and non-linear dynamics to map states from \mathbf{x}_k to \mathbf{x}_{k+1} . To elaborate on this further, we also compare with SINDy and HAVOK, showing the time evolution of the individual components within the states \mathbf{x}_k against the NNs prediction in the Section 5.5.

5.5. Comparison of StNN, FFNN, SINDy, and HAVOK. In this section, we utilize the StNN associated with the lowest validation MSE, where $p = 6$ to compare its performance against the FFNN, SINDy, and HAVOK models, focusing on accuracy and flop counts. For this comparison, we reference a benchmark simulation derived from the Lorenz system as outlined in [13]. For these simulations, we generated trajectories using the Lorenz equations with the same parameters discussed in Section 4.2 that were used to simulate the StNN and FFNN. The system is simulated up to $T = 50$ with a time step of $dt = 0.01$, resulting in a dataset containing 5000 time steps. Initial states $(x, y, z) = (0, 1, 20)$ were used to simulate the system, and the generated



(a) FFNN autoregressive prediction over 600-time steps (b) StNN autoregressive prediction over 600-time steps

FIG. 5. *Time-advanced trajectory prediction using trained FFNN and StNN models over 600-time steps. After training, the FFNN and StNN models are used to predict the future trajectory of the system given an initial condition (red marker). The left plot (a) shows the trajectory predicted by the FFNN (blue), while the right plot (b) shows the trajectory predicted by the StNN (blue). The actual trajectory (orange) serves as a reference for comparison. The results illustrate how well each model captures the system dynamics and maintains accuracy over extended time steps.*

data was split into training and testing sets, with 80% allocated for training and a subset of 600 time steps for testing. We utilized the PySINDy Python package [17] to simulate the SINDy model and the PyDMD Python package [19, 24] to simulate the HAVOK model. Next, we created a 600-step random trajectory for the test, and we provided the FFNN, StNN, SYNDy, and HAVOK with the trajectory’s first initial condition. The 600-step trajectory was then iteratively predicted by running each model 600 times. The predicted values were compared with the actual values to calculate the MSE for 600 steps across three position values. Table 4 and Figure 6 show the accumulated MSE across 600 steps for all the models. The SINDy operator displayed interpretability by presenting an explicit mathematical representation of the dynamics in the form of sparse equations. Its minimal processing overhead makes it ideal for systems with simple, well-defined governing equations. However, the SINDy model has a higher MSE accumulation compared to StNN, especially after 100 time steps.

TABLE 4
Comparison of MSE, flop counts, and parameters among FFNN, StNN, SYNDy, and HAVOK

ML or Data-driven Algorithm	Accumulated MSE at 100 steps	Inference flop counts	Parameters
FFNN	0.288	3960	2073
StNN	0.566	932	408
SINDy	2.452	209	7
HAVOK	16.127	544	1825

In contrast, the StNN offered better performance for complex, nonlinear dynamics. While it required a less computationally intensive training phase than FFNN, the

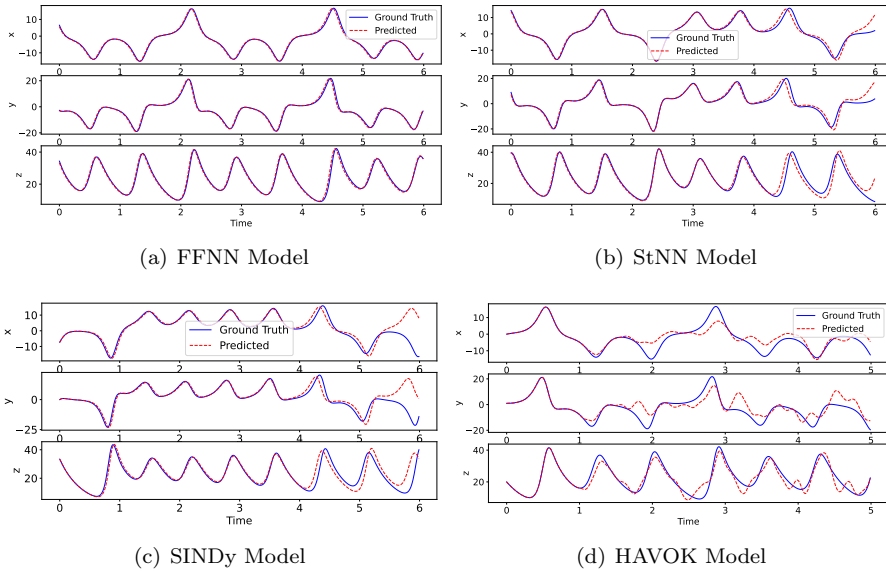


FIG. 6. Comparison of predicted and true trajectories along the x , y , and z axes over 600 time steps for different models. The FFNN (a) and StNN (b) models are the trained machine learning models used for trajectory prediction, while SINDy (c) and HAVOK (d) serve as classical algorithm baselines for comparison. The blue solid lines represent the true trajectory, while the red dashed lines indicate the predicted trajectory. FFNN and StNN show strong alignment with the true trajectory, whereas SINDy exhibits deviations at later time steps. The HAVOK model fails to maintain stability, leading to extreme numerical divergence. This comparison highlights the effectiveness of FFNN and StNN in capturing system dynamics compared to traditional methods.

StNN achieved a smoother and lower cumulative MSE compared to the SINDy and HAVOK operators over the 100-time step trajectory as listed in Table 4.

In terms of computational complexity, SINDy is lightweight, using substantially less memory and flops than StNNs. However, the StNN was shown to be more resilient in precisely simulating the chaotic Lorenz system.

In conclusion, while the FFNN surpasses the StNN in terms of MSE, the StNN has a clear edge in terms of computational efficiency, with fewer flops and weight counts. These qualities make the StNN an attractive choice for use in resource-constrained contexts where efficiency takes importance over absolute error minimization.

6. Conclusions. In this paper, we proposed a low-complexity structured neural network (StNN) for modeling and predicting the evolution of dynamical systems. Our approach uses the Hankel operator to give a structured and computationally efficient alternative to conventional neural networks and data-driven techniques like LEADs, SINDy, and HAVOK. According to numerical simulations based on the Lotka-Volterra model and the Lorenz system, the proposed StNN outperformed other methods in terms of decreasing computer complexity while retaining accurate long-term trajectory predictions. Our findings show that the structured nature of the Hankel operator-based neural network considerably decreases the number of parameters and flop counts while increasing the efficiency of the StNN when compared to conventional techniques. Furthermore, comparisons to baseline approaches, such as FFNN and conventional operator-based techniques, demonstrate StNNs' promise for real-time applications in highly non-linear and chaotic dynamical systems.

Future work will include expanding the StNN framework to higher-dimensional dynamical systems, and utilize the Hankel operator defined through the observation of the state to efficiently solve PDEs.

References.

- [1] E. A. ANTONELO, E. CAMPONOGARA, L. O. SEMAN, J. P. JORDANOU, E. R. DE SOUZA, AND J. F. HÜBNER, *Physics-informed neural nets for control of dynamical systems*, *Neurocomputing*, 579 (2024), p. 127419.
- [2] H. ARBABI AND I. MEZIĆ, *Ergodic theory, dynamic mode decomposition, and computation of spectral properties of the koopman operator*, *SIAM J. Appl. Dyn. Syst.*, 16 (2016), pp. 2096–2126, <https://api.semanticscholar.org/CorpusID:3878613>.
- [3] U. M. ASCHER AND L. R. PETZOLD, *Computer Methods for Ordinary Differential Equations and Differential-Algebraic Equations*, Society for Industrial and Applied Mathematics, Philadelphia, PA, 1998, <https://doi.org/10.1137/1.9781611971392>, <https://epubs.siam.org/doi/abs/10.1137/1.9781611971392>, <https://arxiv.org/abs/https://epubs.siam.org/doi/pdf/10.1137/1.9781611971392>.
- [4] M. ATENCIA, G. JOYA, AND F. SANDOVAL, *Hopfield neural networks for parametric identification of dynamical systems*, *Neural Processing Letters*, 21 (2005), pp. 143–152.
- [5] M. BENZI AND V. SIMONCINI(EDS), *Exploiting Hidden Structure in Matrix Computations: Algorithms and Applications*, Springer, Cham, 2016.
- [6] D. A. BINI, *Matrix structures in queuing models*, in In: Benzi M., Simoncini V. (eds), *Exploiting Hidden Structure in Matrix Computations: Algorithms and Applications*, *Lecture Notes in Mathematics*, 2173, 2016, pp. 65–160.
- [7] D. L. BOLEYA, F. T. LUK, AND D. VANDEVOORDE, *A fast method to diagonalize a hankel matrix*, *Linear Algebra and its Applications*, 284 (1998), pp. 41–52.
- [8] D. S. BROOMHEAD AND R. JONES, *Time-series analysis*, in *Proceedings of the Royal Society of London. Series A, Mathematical and Physical Sciences*, 423(1864), 103–121, 1989.
- [9] B. W. BRUNTON, L. A. JOHNSON, J. G. OJEMANN, AND J. N. KUTZ, *Extracting spatial-temporal coherent patterns in large-scale neural recordings using dynamic mode decomposition*, *Journal of Neuroscience Methods*, 258 (2014), pp. 1–15, <https://api.semanticscholar.org/CorpusID:8635175>.
- [10] S. L. BRUNTON, B. W. BRUNTON, J. L. PROCTOR, E. KAISER, AND J. N. KUTZ, *Chaos as an intermittently forced linear system*, *Nature Communications*, 8 (2016), <https://api.semanticscholar.org/CorpusID:21828799>.
- [11] S. L. BRUNTON, M. BUDIŠIĆ, E. KAISER, AND J. N. KUTZ, *Modern koopman theory for dynamical systems*, *SIAM Rev.*, 64 (2021), pp. 229–340, <https://api.semanticscholar.org/CorpusID:232035467>.
- [12] S. L. BRUNTON AND J. N. KUTZ, *Data-Driven Science and Engineering: Machine Learning, Dynamical Systems, and Control*, Cambridge University Press, Cambridge, 2019.
- [13] S. L. BRUNTON AND J. N. KUTZ, *Data-driven science and engineering: Machine learning, dynamical systems, and control*, Cambridge University Press, Cambridge, 2022.
- [14] S. L. BRUNTON, J. L. PROCTOR, AND J. N. KUTZ, *Discovering governing equations from data by sparse identification of nonlinear dynamical systems*, *Proceedings of the National Academy of Sciences*, 113 (2015), pp. 3932 – 3937.

- [15] J.-F. CAI, E. J. CANDÈS, AND Z. SHEN, *A singular value thresholding algorithm for matrix completion*, SIAM Journal on optimization, 20 (2010), pp. 1956–1982.
- [16] K. K. CHEN, J. H. TU, AND C. W. ROWLEY, *Variants of dynamic mode decomposition: Boundary condition, koopman, and fourier analyses*, Journal of Nonlinear Science, 22 (2012), pp. 887–915.
- [17] B. DE SILVA, K. CHAMPION, M. QUADE, J.-C. LOISEAU, J. KUTZ, AND S. BRUNTON, *Pysindy: A python package for the sparse identification of nonlinear dynamical systems from data*, Journal of Open Source Software, 5 (2020), p. 2104, <https://doi.org/10.21105/joss.02104>, <https://doi.org/10.21105/joss.02104>.
- [18] J. DEMMEL, *Applied Numerical Linear Algebra*, SIAM, Philadelphia, PA, 1997.
- [19] N. DEMO, M. TEZZELE, AND G. ROZZA, *Pydmd: Python dynamic mode decomposition*, Journal of Open Source Software, 3 (2018), p. 530.
- [20] G. H. GOLUB AND C. F. VAN LOAN, *Matrix Computations*, The Johns Hopkins University Press, Baltimore, 4th ed., 2013.
- [21] I. GOODFELLOW, Y. BENGIO, AND A. COURVILLE, *Deep Learning*, MIT Press, Cambridge, MA, 2016. <http://www.deeplearningbook.org>.
- [22] G. HEINIG, *Fast and superfast algorithms for hankel-like matrices related to orthogonal polynomials*, in Vulkov L., Yalamov P., Waśniewski J. (eds) Numerical Analysis and Its Applications, Lecture Notes in Computer Science 1988, Springer, Berlin, Heidelberg, 2001.
- [23] G. HEINIG AND K. ROST, *Algebraic Methods for Toeplitz-Like Matrices and Operators*, Akademie-Verlag, Berlin, and Birkhauser Basel, Boston, MA, 1984.
- [24] S. M. ICHINAGA, F. ANDREUZZI, N. DEMO, M. TEZZELE, K. LAPO, G. ROZZA, S. L. BRUNTON, AND J. N. KUTZ, *Pydmd: A python package for robust dynamic mode decomposition*, arXiv preprint arXiv:2402.07463, (2024).
- [25] S. JI AND J. YE, *An accelerated gradient method for trace norm minimization*, in Proceedings of the 26th annual international conference on machine learning, 2009, pp. 457–464.
- [26] J.-N. JUANG AND R. S. PAPPA, *An eigensystem realization algorithm for modal parameter identification and model reduction. [control systems design for large space structures]*, 1985, <https://api.semanticscholar.org/CorpusID:9239187>.
- [27] T. KAILATH, *Linear Systems*, Pearson, India, 2016.
- [28] T. KAILATH AND A. SAYED, *Fast Reliable Algorithms for Matrices with Structure*, SIAM Publications, Philadelphia, USA, 1999.
- [29] J. N. KUTZ, S. L. BRUNTON, B. W. BRUNTON, AND J. L. PROCTOR, *Dynamic mode decomposition: data-driven modeling of complex systems*, SIAM, Philadelphia, PA, 2016.
- [30] B. LUSCH, J. N. KUTZ, AND S. L. BRUNTON, *Deep learning for universal linear embeddings of nonlinear dynamics*, Nature communications, 9 (2018), p. 4950.
- [31] F. D. MARCO, *Torch-levenberg-marquardt: A pytorch implementation of the levenberg-marquardt algorithm*, 2025, <https://github.com/fabiodimarco/torch-levenberg-marquardt>. Accessed: 2025-01-21.
- [32] I. MEZIĆ, *Spectral properties of dynamical systems, model reduction and decompositions*, Nonlinear Dynamics, 41 (2005), pp. 309–325, <https://api.semanticscholar.org/CorpusID:37635186>.
- [33] V. OLSHEVSKY, *Fast algorithms for structured matrices: Theory and applications*, in Contemporary Mathematics, 323, 2003.
- [34] V. Y. PAN, *Structured Matrices and Polynomials: Unified Superfast Algorithms*, Birkhauser/Springer, Boston/New York, 2001.

- [35] S. M. PERERA AND I. S. KOTSIREAS, *A low-complexity algorithm to search for legendre pairs*, Linear Algebra and its Applications, (2025), <https://doi.org/https://doi.org/10.1016/j.laa.2025.01.010>, <https://www.sciencedirect.com/science/article/pii/S0024379525000102>.
- [36] S. M. PERERA, L. LINGSCH, A. MADANAYAKE, AND L. BELOSTOTSKI, *A low-complexity algorithm to digitally uncouple the mutual coupling effect in antenna arrays*, in in review, the Journal of Computational and Applied Mathematics, 2023.
- [37] S. M. PERERA, L. LINGSCH, A. MADANAYAKE, S. MANDAL, AND N. MASTRONARDI, *Fast dvm algorithm for wideband time-delay multi-beam beamformers*, the IEEE Transactions on Signal Processing, 70 (2022).
- [38] J. L. PROCTOR, S. L. BRUNTON, AND J. N. KUTZ, *Dynamic mode decomposition with control*, SIAM J. Appl. Dyn. Syst., 15 (2014), pp. 142–161.
- [39] P. RAJENDRA AND V. BRAHMAJIRAO, *Modeling of dynamical systems through deep learning*, Biophysical Reviews, 12 (2020), pp. 1311–1320.
- [40] P. J. SCHMID, *Dynamic mode decomposition of numerical and experimental data*, Journal of Fluid Mechanics, 656 (2010), p. 5–28, <https://doi.org/10.1017/S0022112010001217>.
- [41] P. J. SCHMID AND P. ECOLE, *Dynamic mode decomposition of numerical and experimental data*, Journal of Fluid Mechanics, 656 (2008), pp. 5 – 28, <https://api.semanticscholar.org/CorpusID:11334986>.
- [42] G. STRANG, *Linear Algebra and Learning from Data*, Wesley Cambridge, MA, 2019.
- [43] K. SUZUKI, H. MORI, AND T. OGATA, *Motion switching with sensory and instruction signals by designing dynamical systems using deep neural network*, IEEE Robotics and Automation Letters, 3 (2018), pp. 3481–3488.
- [44] J. W. THOMAS, *Numerical Partial Differential Equations: Finite Difference Methods*, Springer-Verlag, New York, 1995, <https://doi.org/10.1007/978-1-4899-7278-1>, <https://doi.org/10.1007/978-1-4899-7278-1>.
- [45] K.-C. TOH AND S. YUN, *An accelerated proximal gradient algorithm for nuclear norm regularized linear least squares problems*, Pacific Journal of optimization, 6 (2010), p. 15.
- [46] L. N. TREFETHEN AND I. D. BAU, *Numerical Linear Algebra*, SIAM, Philadelphia, PA, 1997.
- [47] A. P. TRISCHLER AND G. M. D’ELEUTERIO, *Synthesis of recurrent neural networks for dynamical system simulation*, Neural Networks, 80 (2016), pp. 67–78.
- [48] J. H. TU, C. W. ROWLEY, D. M. LUCHTENBURG, S. L. BRUNTON, AND J. N. KUTZ, *On dynamic mode decomposition: Theory and applications*, Journal of Computational Dynamics, 1 (2014), pp. 391–421, <https://doi.org/10.3934/jcd.2014.1.391>.
- [49] Y. YIN, I. AYED, E. DE BÉZENAC, N. BASKIOTIS, AND P. GALLINARI, *Leads: Learning dynamical systems that generalize across environments*, 2021, <https://proceedings.neurips.cc/paper/2021/file/3df1d4b96d8976ff5986393e8767f5b2-Paper.pdf>.